# Time-Resolved Dielectric Loss for Characterization of Photoconductive and Photocatalytic Materials[†]

**M. R. V. Sahyun***

*Department of Chemistry, University of Wisconsin, Eau Claire, Wisconsin 54702*

The purpose of this tutorial review is to illustrate the use of time-resolved dielectric loss (TRDL) and analysis of TRDL data on photoconductive materials for electrophotographic applications, as well as on photocatalytic imaging processes. Systems studied in our laboratories include particulate CdS for Canongraphic imaging and CdS powder dispersed in a xylene solution of phenylhydrazine, as a model for a photorecptor with separated charge generation and charge transport function. A study on prototypical molecular charge generation media is also reviewed, as is recent work on the characterization of $TiO_2$, a prototypical photocatalyst of demonstrated imaging utility.

Journal of Imaging Science and Technology 41: 127–134 (1997)

## Introduction

The theory and instrumentation of dielectric loss measurement and time-resolved microwave photoconductivity have been described elsewhere.[1,2] These techniques provide information on the concentration and mobility of charge carriers in photoresponsive solids. Relaxation processes of interest in the characterization of photoconductive and photocatalytic materials, e.g., receptors for electrophotography, usually occur in the microsecond to millisecond regime, hence it is necessary to probe them using microwave frequencies, that allows nanosecond resolution.[3,4] Under these conditions the two methods become, essentially, one and the same. We accordingly use the term *time-resolved dielectric loss* (TRDL). Theory and interpretation of TRDL measurements in the microwave frequency domain have been described by Warman,[5] with reference to ionic relaxation following pulse radiolysis, and by Deri and Spoonhower,[4] within the specific context of silver halide science.

One of the substrates whose photophysics was studied earliest using TRDL was single crystal CdS.[6–8] Initially, however, steady-state microwave photoconductivity tended to be employed for determining electrophotographic characteristics of II-VI materials in pigment form.[9,10] In this technique, a pulsed light source is used, with lock-in detection of variations in the power density in the microwave cavity containing the sample. These studies on CdS became the models for subsequent work characterizing other bulk and particulate materials.

Photocatalytic semiconductors are of interest both for their direct utility in several nonconventional imaging processes[11–13] and also as models for less directly probed silver halide systems.[14,15] In many cases their behavior in an aqueous environment is of specific interest. This complicates the use of TRDL owing to the high microwave absorptivity of water. Various strategies have been employed to obviate this difficulty, including special cell design for use with semiconductor electrodes[16] and use of a thin-film flow cell for probing colloidal dispersions.[17] More recently, aqueous media have been studied with superior signal-to-noise ratio, but limited temporal resolution, using radio frequency TRDL.[18]

Growing interest in nanoparticulate materials for imaging and electronics applications as well as photocatalysis[18] encourages extension of TRDL to materials in this size range. Its application is not stratighforward, however, owing to the issue of sample depolarization, i.e., limitation of the microwave energy loss, $\Delta P \propto Ed$ (where ω is the microwave frequency, $E$ is the electric field strength, and $d$ is the charge carrier displacement distance) owing to particle size limitation of $d$. Thus

$$d = \mu E/\omega, \tag{1}$$

where μ is the Hall mobility for the majority carriers, e.g., 500 cm²/V-s for electrons in CdS. Typically $E$ in microwave cavities is of the order of a few V/cm, and ω is 10 to 40 GHz from commercially available microwave sources. These values for the experimental parameters yield $d \leq 25$ Å, which represents the lower limit on the particle size of the photoconductive material that can be probed by TRDL. When radio-frequency TRDL is used, however, ω may be ~ 160 MHz,[18] so that $d = 0.15$ μm. The radio-frequency approach is thus suspect for application to nanoparticulate materials.

The focus of this review is to illustrate the analysis of TRDL data on particulate photoconductive materials for

---

Original manuscript received September 10, 1996.

* IS&T Fellow and Senior Member.

[†] Presented at the Symposium: "Physical Methods for Characterizing Imaging Materials and Processes", at the 49th Annual Conference, IS&T, Minneapolis, MN, May 20, 1996.

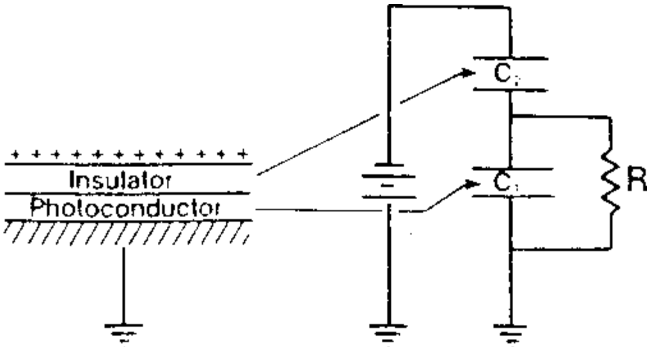

**Figure 1.** Equivalent circuit diagram of a typical Canongraphic detector (after Ref. 21b). See text for a detailed description of the Canongraphic process.

electrophotographic applications and for photocatalytic imaging, drawing on examples from our own work and the literature.

## Experimental

In examples from our own work carried out in the Information, Imaging and Electronics Sector Laboratories of 3M, microwave energy loss was measured with a commercial Micro-Now model 815R microwave spectrometer. This instrument utilizes an X band, rectangular cavity, operating in the TE103 mode. Microwave field frequency is tunable in the range of 9 ± 2 GHz to allow a temporal resolution of ~ 100 ns.[4] A Gen-Rad Strobotac® xenon flash lamp with pulse width of ~ 2 µs was normally used for flash irradiation of the samples. This source operated at ~ 10 Hz to allow for collection and computer averaging of multiple transients, displayed on a 100-MHz storage oscilloscope. For variable temperature studies, samples were probed in a jacketed quartz cell and thermostatted in a dry helium stream, which had been heat exchanged with a bath at the appropriate temperature. Other specific experimental details are provided in the references cited.

## Case Histories.

***CdS powders.*** Xerographic discharge characteristics of II-VI powder-insulating binder composite photoconductors tend to be dominated by the electrical properties of interparticle contacts in the mixture.[19] Spatially discontinuous discharge rates may thus contribute significant levels of noise to the images captured in this manner. On the other hand, pigment-binder composite layers have proven very useful in photoconductor–insulator constructions, e.g., in the Canongraphic engines[20] or in electroradiographic schemes[21] where the shot noise is intrinsically coarser.

The equivalent circuit[21b] of a Canongraphic detector is shown in Fig. 1. This image sensor comprises a bilayer photoconductor–insulator construction, whose photoresponse may be either capacitive or conductive, i.e., either $C_1$ or R in Fig. 1 may vary on exposure of the device to light. The photoconductor is typically a composite of a particulate photoconductor dispersed in an insulating polymer binder. Sensitivity of the device depends on the voltage change, $\Delta V = V_0 - V_\infty$, where $V_0$ is the voltage applied across the device in the dark, and $V_\infty$ is the voltage drop across the insulator, i.e., the component of the originally applied voltage remaining after discharge of the composite photoconductor. It thus corresponds to the voltage drop across the leaky capacitor, $C_1$, corresponding to the composite photoconductor in the dark.

A variety of CdS powders for a Canongraphic application were screened by the TRDL method.[22,23] A typical TRDL response is shown in Fig. 2. It exhibits four features:

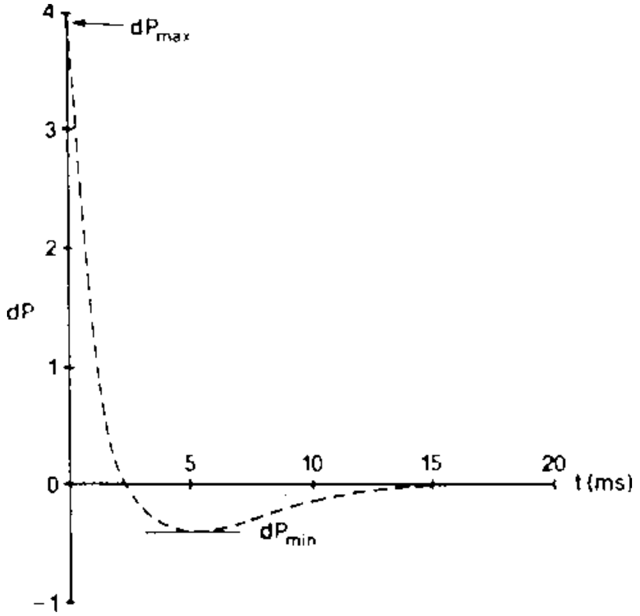

**Figure 2.** Representative TRDL oscillograph (idealized) for CdS powder (after Ref. 22).

1. $\Delta P_{\max}$, the maximum microwave power loss, obtained immediately at the end of the light pulse;
2. $\tau_1$, the exponential decay lifetime of the power loss signal;
3. $\Delta P_{\min}$, the "overshoot" of the baseline corresponding to a physical situation in which the initially relaxed sample contains a lower concentration of mobile charge carriers than at equilibrium.[6]
4. $\tau_2$, the lifetime for return to the equilibrium power density.

We will examine the interpretation of each of these features, in turn.

The maximum power loss, $\Delta P_{\max}$, reflects both the number of carriers produced, as well as their mobility. Given that the Hall mobility is a more or less constant characteristic of the material, variation of $\Delta P_{\max}$ with sample preparation, exposure conditions, etc., should reflect the relative efficiency of free-electron generation in the conduction band of the CdS sample. The temperature dependence of $\Delta P_{\max}$ obtained under conditions of irradiation with light filtered to pass only wavelengths beyond the band edge (530 nm) for a representative Cu-doped CdS sample is shown as an Arrhenius plot in Fig. 3. We estimated an activation energy, $\Delta E^a{}_{\mathrm{obs}}$ of 0.175 eV. It can be shown[22] that

$$\Delta E^a{}_{\mathrm{obs}} = \Delta E^a{}_{\mathrm{n}} - \Delta E^a\,(\tau_1), \qquad (2)$$

where $\Delta E^a{}_n$ is the activation energy for free-electron generation and $\Delta E^a(\tau_1)$ is the activation energy associated with the signal decay process, as described by $\tau_1$. We found, as discussed later, that $\Delta E^a(\tau_1) = -0.035$ eV, so that $\Delta E^a{}_n = 0.22$ eV.

Free-carrier generation in the CdS photoconductor is thus thermally activated. We assigned this activation to intermediacy of a subconduction band donor level, later[23] shown to be a sulfide ion vacancy state.[24] From the point of view of technological development, it was important to understand that this activation barrier is not associated with, e.g., interparticle contacts in the composite photoconductor but was a characteristic of the II-VI material itself.

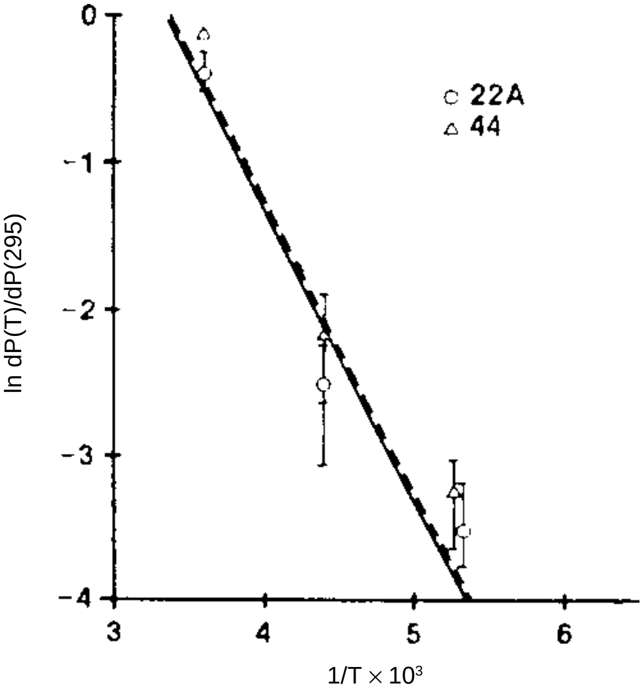

**Figure 3.** Arrhenius plot of TRDL signal, $\Delta P_{max}$, for Cu-doped CdS (data from Ref. 22; circles correspond to green light exposure and triangles correspond to red light exposure).

We turn now to the interpretation of the power loss decay kinetics. Essentially equivalent, general reaction schemes for the trapping and recombination of photogenerated charge carriers in doped II-VI materials have been proposed by Collier and coworkers[8] and by Düssel and Boer.[25] A steady-state analysis of a kinetic treatment of these models[22,23] shows that

$$1/\tau_1 = k_3K[\mathrm{Cu(I)}] \qquad (3)$$

where $K$ is the equilibrium constant for the Coulombic binding of photoholes to the Cu(I) centers, substitutional for Cd(II), and $k_3$ is the pseudo-first-order rate constant for the chemical reaction

$$\mathrm{Cu(I)}\cdot p \rightarrow \mathrm{Cu(II)}, \qquad (4)$$

where Cu(I) · $p$ designates the holes electrostatically bound to the Cu(I) center. It follows that

$$n_0 \propto 1/k_3K[\mathrm{Cu(I)}] \qquad (5)$$

where $n_0$ is the concentration of free photoelectrons at $t$ = 0, i.e., $\Delta P_{max}$, whereby Eq. 2 is obtained. The prediction of Eq. 3 has been verified by Collier.[8]

The message in this analysis is that even though, to a first approximation, only free photoelectron dynamics are probed in the TRDL experiment, what we actually measured was the rate of a hole-trapping process, i.e., the rate-limiting step in recombination was the rate at which oxidation of Cu(I) centers to Cu(II) sets the traps responsible for recombination.

The Arrhenius analysis of $\tau_1$, shown in Fig. 4, leads to a negative activation energy, $\Delta E^a(\tau_1) = -0.035$ eV, where from Eq. 3

$$\Delta E^a(\tau_1) = \Delta E^a(k_3) + \Delta H(K), \qquad (6)$$

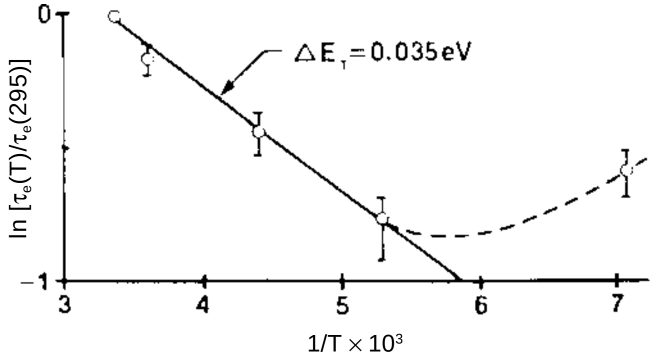

**Figure 4.** As Fig. 3, for $\tau_1$ (data from Ref. 22).

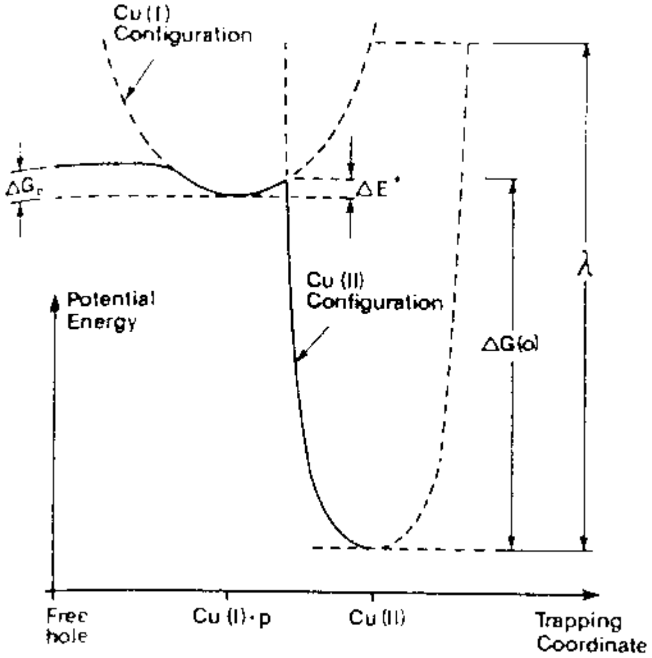

**Figure 5.** Double minimum potential energy surface for hole trapping at Cu(I) center in Cu-doped CdS (after Ref. 22).

where $\Delta H(K)$ is the enthalpy associated with the Coulombic binding of the hole to the Cu(I) center. If binding is exergonic, $\Delta H(K) < 0$; for $|\Delta H(K)| > \Delta E^a(k_3)$, then $\Delta E^a(\tau_1) < 0$. These considerations reveal that hole trapping at the Cu(I) centers occurs on a double minimum potential energy surface, as shown in Fig. 5. A similar double minimum potential surface has been demonstrated in photoluminescence studies for hole trapping at Ag(I) centers in the common green-emitting phosphor Zn(Cd)S:Ag.[26]

We determined by control experiments that the "overshoot" designated $\Delta P_{min}$ in Fig. 2 was not an electronic artifact, but another characteristic of the materials. We accordingly found that a parameter

$$\alpha = -(\Delta P_{max}/\Delta P_{min}) \qquad (7)$$

correlated with $\Delta V$ for Canongraphic response (Fig. 6). We can then identify the process characterized by $\tau_2$ with thermalization of deep-trapped electrons, which restores the dark equilibrium concentration of conduction band electrons. Accordingly, $\Delta P_{min}$ is a measure of the density of states of deep traps near the Fermi level of $n$-type CdS. Existence of a large density of such states can confer metal-like

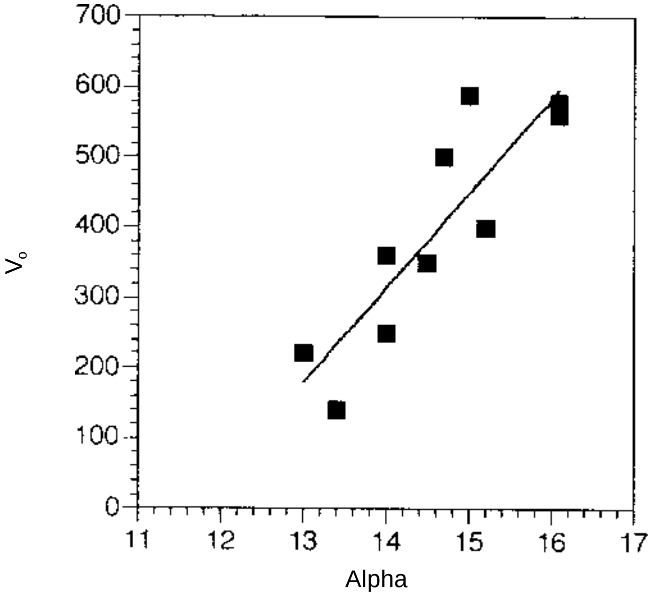

**Figure 6.** Use of α (Eq. 7) as a figure of merit for prediction of Canongraphic performance (as $\Delta V$) (after Ref. 22).

**TABLE I. Phenylhydrazines (Y-Phnhnh$_2$) Used to Mediate Surface Recombination on II-VI Powders**

| Compound | | σ | Ref. |
|---|---|---|---|
| Y = | *para*-methoxy | –0.78 | 36a |
| | *para*-methyl | –0.31 | 36a |
| | H | 0 | 35 |
| | *para*-chloro | +0.11 | 36a |
| | *meta*-methoxy | +0.25 | 37 |
| | *meta*-chloro | +0.47 | 37 |
| | *meta*-fluoro | +0.52 | 37 |

properties on the semiconductive solid.[27] Accordingly, increasing $|\Delta P_{\min}|$, i.e., decreasing α, reflects decreasing capacitance, $C_2$, and, perhaps, increasing leakiness ($1/R$) as well (cf. Fig. 1).

***Interfacial Electron Transfer***. The low mobilities of the charge carriers in organic photoconductors in which field-dependent hopping conductivity usually predominates[28] effectively preclude the use of TRDL to study their photophysics. Practical electrophotography with organic photoconductors generally employs two component photoreceptors: a charge-generating phase is present as a separate layer adjacent to the organic charge transport layer,[29] or the charge-generating material is present in the form of a particulate dispersion within the charge transport phase.[29,30] The charge transport phase itself is usually a molecularly doped polymer, i.e., solid solution, and the charge-generating phase may be either organic or inorganic. Surprisingly, the physics of charge generation appears to exhibit little dependence on the chemical composition of the charge-generating material.[29b]

Modeling of the charge generation process requires the electron–hole ambipolar separation distance, $r$, at the beginning of diffusion as a fitting parameter.[29b,c] Our studies of a model system were therefore undertaken to demonstrate the ability of the TRDL technique to provide a solution to this problem. Since photoconductor choice is not critical, we used an undoped, electronic grade CdS,[31,32] which exhibits only binary recombination in the absence of surface treatment, ZnO,[31] and Zn(Cd)S, which required surface metallization with Pd in order for interfacial charge transfer processes to become observable.[33] Such deposition of catalytic metal microislands on the surface of a semiconductor powder to facilitate interfacial electron transfer is common practice in semiconductor electrode technology[34a] and heterogeneous photocatalysis.[34b,c] As the hole accepting species, i.e., the prototypical charge transport agent, we chose a series of phenylhydrazines (Y-ϕ-NHNH$_2$, where Y is a substituent on the phenyl ring). A list of the phenylhydrazines and their Hammett substituent coefficients (see below) is given in Table I.

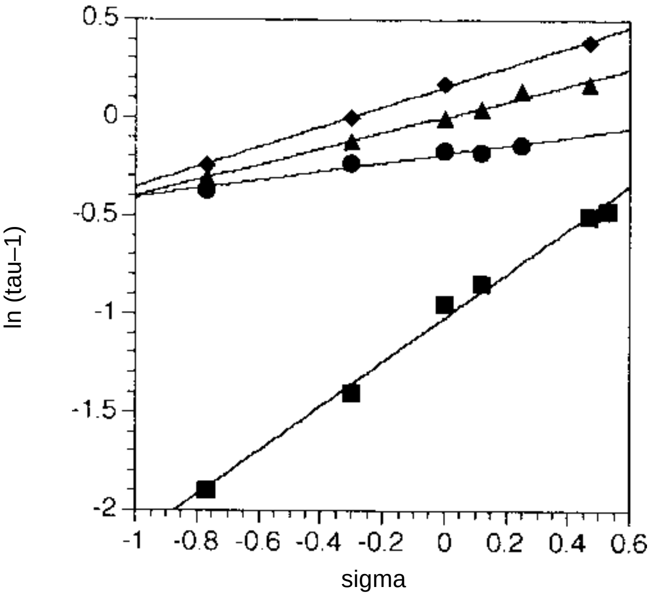

**Figure 7.** Hammett ρσ plot for recombination lifetime (as ln $\tau_1$) in CdS (at various temperatures) and Zn(Cd)S:Pd with adsorbed substituted phenylhydrazines (data from Refs. 31 and 32): lower line, Zn(Cd)S at room temperature; upper three curves, CdS at (top to bottom) 0°, 23°, and 45°.

The CdS powder was dispersed in xylene, rather than a dielectric polymer, to facilitate the TRDL measurement, and the phenylhydrazines were dissolved in the xylene at ~ 0.1 M. Thus a fluid solution of phenylhydrazine in xylene was substituted for the solid solution of charge transport agent in polymer typically used in electrophotographic receptors. The concentration of phenylhydrazine employed was too dilute for charge transport away from the CdS particles to compete with surface recombination.

$$\mathrm{PhNHNH_2 + p^+ \rightarrow PhNHNH_2^{\cdot +}} \tag{8a}$$

$$\mathrm{PhNHNH_2^{\cdot +}} + e^- \rightarrow \mathrm{PhNhNH_2} \tag{8b}$$

In this system we could vary the energetics of charge transfer by variation of the phenylhydrazine ring substituent, Y, expressed in terms of the Hammett σ parameter.[35] Although a variety of parameters have been tabulated, in this application we used the one usually designated ($\sigma^+$)[36] for *para*-substituents and ($\sigma_I$)[37] for the *meta*-substituents (see Table I).

In the presence of the phenylhydrazine, the decay of the TRDL signal for all the photoconductors became singly exponential, with lifetime $\tau_1$; in no case was overshoot, i.e., $\Delta P_{\min}$ as in Fig. 2, observed. We interpret these results in all cases in terms of interfacial recombination mediated by adsorbed phenylhydrazine according to Eqs. 8a and 8b. Thus $\tau_1$ is the reciprocal of the pseudo-first-order recombination rate constant. It is not clear, however, whether Eq. 8a or 8b is rate determining in such recombination.

Accordingly we plotted ln $\tau_1$ versus σ for recombination on CdS at three temperatures and on Zn(Cd)S:Pd at room temperature as in Fig. 7. From these plots, the reaction

**TABLE II. Hammett Analysis of Phenylhydrazine Mediated Surface Recombination on Particulate Ii-Vi Semiconductors.**

| $T$ (°C) | $\rho$ | $r^a$ | ln $\tau$ (ms, Y = H) |
|---|---|---|---|
| CdS: | | | |
| 0 | –0.49 | 0.997 | 0.165 |
| 23 | –0.39 | 0.992 | -0.020 |
| 42 | –0.22 | 0.969 [b] | -0.127 |
| Zn(Cd)S:Pd: | | | |
| 23 | –1.17 | 0.997 | -0.98 |

[a] Correlation coefficient.

[b] Excluding data points for *meta*-chloro- and *meta*-fluorophenylhydrazines (most positive σ's)

constants, ρ, were obtained as the negative of the slopes of the least-squares fits to the experimental data. These parameters are given in Table II. The usual interpretation of Hammett reaction constants[35,36b] suggests that the sign of the ρ values is diagnostic for one-electron oxidation of the phenylhydrazine to be rate determining, i.e., Eq. 8a. This may not, in fact, be the case.

The Hammett treatment is a special case of a linear free-energy correlation, in which σ is a predictor of the free-energy change, $\Delta G$, of the reaction;[35] thus

$$\rho \propto (d\Delta G^{\neq}/d\Delta G), \qquad (9)$$

where $\Delta G^{\neq}$ is the Gibbs free energy of activation of the rate determining step. We expect the substituent parameter, σ, to reflect the ionization potential of the phenylhydrazine.[36b]

According to Marcus electron transfer theory[38] the value of the derivative in Eq. 9 will be greater than zero for the so-called Marcus normal regime, but negative in the Marcus inverted regime. Hence the physical interpretation placed on the sign of ρ will also depend on whether the process occurs energetically in the Marcus normal or the Marcus inverted regime. This can be seen by differentiation of the Marcus Eq. as usually written:

$$\Delta G^{\neq} = (\lambda/4)(1 + \Delta G/2\lambda)^2, \qquad (10)$$

so that

$$d\Delta G^{\neq}/d\Delta G = 1/2 + \Delta G/\lambda \qquad (11)$$

where λ is the so-called reorganization energy. Thus

$$\begin{aligned} d\Delta G^{\neq}/d\Delta G &= 0 \text{ for } \lambda = -\Delta G, \\ d\Delta G^{\neq}/d\Delta G &\geq 0 \text{ for } \lambda > -\Delta G, \qquad (12) \\ d\Delta G^{\neq}/d\Delta G &\leq 0 \text{ for } \lambda < -\Delta G. \end{aligned}$$

The reorganization energy is a free energy which can be divided into enthalpic and entropic components, $\lambda_h$ and $\lambda_s$, respectively.[39] If there exists a temperature, called the *compensation temperature*, $T_{\text{comp}}$, at which $d\Delta G^{\neq}/d\Delta G = 0$, then

$$-\Delta G = \lambda_h - T_{\text{comp}}\lambda_s \qquad (13)$$

and

$$d\lambda/dT = -\lambda_s \qquad (14a)$$

$$d\Delta G/dT = \lambda_s \qquad (14b)$$

Extrapolation of the data of Table II for recombination on CdS yields $T_{\text{comp}} = (80 \pm 3)^0$, as shown in Fig. 8.

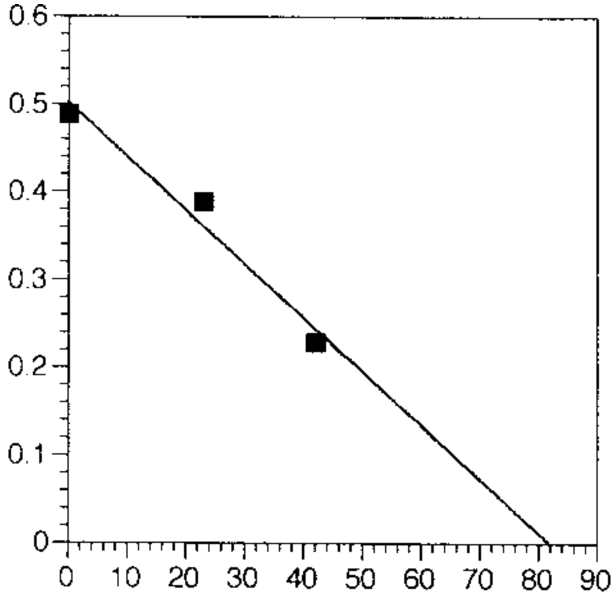

**Figure 8.** Temperature dependence of ρ values for phenylhydrazine-mediated CdS surface recombination estimated from plots of Fig. 7.

Differentiation of the Marcus Eq. with respect to $T$ yields in approximate form

$$d\Delta G^{\neq}/dT = (1/4)(d\lambda/dT) + (1/2)(d\Delta G/dT), \qquad (15)$$

which at $T = T_{\text{comp}}$ reduces (by insertion of Eqs. 14a and 14b) to

$$d\Delta G^{\neq}/dT = (1/4)\lambda_s. \qquad (16)$$

From the data of Table II with $T_{\text{comp}} = 80°$, we estimated $\lambda_s = +\ 67\ \text{JK}^{-1}\text{mol}^{-1}$ for phenylhydrazine mediated surface recombination on CdS. Thus λ is counter-proportional to temperature and $(\partial\Delta G^{\neq}/\partial\lambda) > 0$. Since (again by differentiation of Eq. 10).

$$(\partial\Delta G^{\neq}/\partial\lambda) = (1/4)[(\lambda^2 - \Delta G^2)/\lambda^2], \qquad (17)$$

$|\Delta G| < |\lambda|$, which, given the boundary condition that $\Delta G = -\lambda$ at $T = T_{\text{comp}}$ and Eq. 15, which requires that for $d\Delta G^{\neq}/dT > 0$ and $d\lambda/dT < 0$ that $d\Delta G/dT > 0$ (and also $dDG/dT > |d\lambda/dT|$),

$$\Delta G > -\lambda\ , \qquad (18)$$

the reaction occurs in the Marcus normal regime and, in accord with conventional wisdom, Eq. 8a must be rate determining. The lesson from this exercise is that it is critical to know whether an electron transfer process is occurring energetically in the Marcus normal or the Marcus inverted regime, *before* attaching physical significance to the sign or magnitude of the slope of a linear free energy correlation.

Inequality 18 strongly suggests that Eq. 8a describes merely the limiting step of a multiphonon transition[40] by which holes are trapped at the surface state formed by adsorption of phenylhydrazine on the semiconductor. The larger absolute value of ρ (Table II) for the Pd deposited Zn(Cd)S implies a smaller absolute value of $\Delta G$ for this case. This interpretation is consistent with the multistep trapping model, with the Pd microislands providing more closely spaced levels than available in the undoped CdS.

From the point of view of interfacial charge transfer, i.e., practical electrophotography, it would be desirable for Eq. 8b to be rate limiting. Thereby hole transfer away from the charge-generating particle could compete more effectively with surface recombination.

We use Dogonadze's expression[41] for the nonadiabatic electron transfer frequency,

$$\omega = (k_bT/h)\kappa \exp(-\Delta H^{\neq}/k_bT) \exp(\Delta S^{\neq}/k_b) \qquad (19)$$

with experimental estimates of the activation parameters[31] and $\omega = \tau^{-1}$, to evaluate the transmission coefficient, κ, where[42]

$$\kappa = \exp[-(r - r_0)/a]. \qquad (20)$$

Using the usual values of 6 Å for the close-contact distance, $r_0$, and $a = 1$ Å, we now reach our intended goal of estimating the ambipolar electron–hole separation distance at the beginning of carrier drift, and estimate $r = 20$ Å for CdS. Physically this estimate corresponds to the thickness of the interfacial layer, i.e., the depletion zone in the photoconductive particle across which electron–hole separation occurs.

***Intramolecular Charge Separation***. Molecular charge-generating systems have been used with organic photoconductors, particularly polyvinylcarbazole (PVK). Smit and Warman[43] have studied a series of such charge generating compounds of the structure

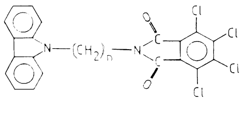

I

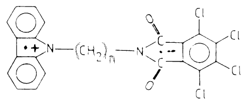

I*(ICT)

in organic solution using TRDL. From the point of view of the development of the TRDL technique, this report is extremely important because it demonstrates the method's utility for probing phenomena at the molecular level. Accordingly these authors have been able to demonstrate formation of both singlet and triplet radical pair charge-transfer states (ICT), and measure the rate of formation of the latter from the former, as well as the recombination-limited lifetimes of both states. Intramolecular charge separation occurs within 25 ps of photoexcitation of ***I***, with spin relaxation occurring on the timescale of ~ 500 ns in nonpolar media.

In the unpaired spin state of ***I*** the charges are more tightly bound, and the excited state is more susceptible to deactivation by reaction with atmospheric oxygen, compared to the spin-paired, charge transfer state. In the representative charge transport material polyvinyl carbazole, PVK,[44] the limiting hole mobility, $\mu = 5 \times 10^{-6}$ cm$^2$V$^{-1}$s$^{-1}$, at an electrostatic field strength, $E = 10^6$ V cm$^{-1}$, establishes a saturation drift velocity of ~ 5 cm s$^{-1}$. The volume-average hopping radius, $r$, has been estimated[45] from several data sets as ~ 30 Å in PVK. The charge separation efficiency, Φ, is accordingly

$$\Phi = \mu E/(\mu E + r\tau^{-1}), \qquad (21)$$

about 0.89 using the spin relaxation lifetime for ***I*** for τ. This estimate indicates that electrophotographic charge generation in a system based on a molecular charge generating component, e.g., ***I***, can be very efficient. Note that compounds such as ***I***, however, are only photoresponsive in the near-ultraviolet region, hence they are only useful as models of practical charge-generating molecules.

***Photocatalytic Imaging***. Several imaging processes are described in which image-wise irradiation of a photoconductor leads to reduction of noble metal ions, thereby forming nuclei for subsequent physical development.[13] Collectively we can term these processes *photocatalytic imaging*. When $TiO_2$ is used as the photoconductor it allows postexposure treatment with the metal ion in solution, rather than requiring exposure in the presence of the metal ion. Thus exposure of $TiO_2$ appears to form a *latent image*, the nature of which has not been characterized. A more recent report[11b] suggests that the silver halide component in thermally developable photomaterials based on juxtaposed silver halide and silver carboxylate phases acts similarly as a photocatalyst to reduce silver ions from the silver carboxylate phase to form development centers. In support of this view it can be pointed out that photothermographic imaging is feasible with similar media in which $TiO_2$ is substituted for the silver halide.[11a,12]

Heterogeneous photocatalysis may also be of importance to the imaging industry insofar as photocatalytic reduction of silver on $TiO_2$ has been shown to be a viable route to silver recovery from conventional photographic processing effluents.[46,47] Nanoparticulate $TiO_2$ appears to be the photocatalyst of choice for both photocatalytic imaging and silver recovery applications. It exists in two crystallographic forms, anatase and rutile; anatase is usually preferred for imaging applications.

Chemical studies of the photocatalytic deposition of silver on $TiO_2$ conducted using large particles of the photocatalyst, e.g., single crystals of photoconductive electrodes,[48] led to an electrochemical model for the process. Fleischauer, et al.[48a] assumed electron transfer from the conduction band under flatband conditions to adsorbed silver ion, without intervention of deep-trapped electron states. On the other hand, laser flash spectroscopy[49,50] of nanocrystalline $TiO_2$ preparations has demonstrated that photoelectrons may be trapped "immediately" on generation, but free photoholes in some cases have a longer lifetime, leading to free hole–trapped electron recombination. The deep-trapped photoelectrons are identified with surface Ti(III) states.[50] Quantum yield studies of silver deposition on a nanoparticulate $TiO_2$ preparation typically advocated for silver recovery technology, actually a mixture of anatase and rutile forms, have, however, specifically excluded such recombination as a significant loss process.[46]

Photophysics of nanoparticulate $TiO_2$ have been probed by TRDL[51,52] to resolve these seeming contradictions. Adaptation of the technique to study of nanoparticulate materials immediately raises the issue of space charge limitation of the TRDL response. Reference to Eq. 1 leads to the conclusion that under conditions typical of TRDL practice, particles as small as 25 Å may be probed. The TRDL results of Martin and coworkers[52] on an anatase $TiO_2$ preparation that is particularly active for photocatalytic deposition of silver[53] demonstrated that a population of mobile photoelectrons appears to persist for up to several microseconds following flash exposure of a sol of the particles. From temperature dependence of $dP_{\max}$ (as described earlier in connection with studies on CdS) these authors inferred that a trap of thermal depth $\Delta E_t = 0.25$ eV below the conduction band intervened in generation of free electrons. Our own results[53] on the same material indicate that the trapping equilibrium is established within 5 ns. The traps may be identified with Ti(III) states observed spectroscopically in similar materials.[49,50]

It is important to the interpretation of the results, however, to realize that application of the microwave field creates a nonequilibrium situation. The concentration of free carriers, $n_f$, relative to trapped photoelectrons, $n_t$, under conditions of the TRDL experiment can then be estimated from the Poole–Frenkel model of field-induced detrapping.[54] Accordingly

$$n_f/n_t = \exp[\,-(\Delta E_t - \beta E^{0.5})/k_bT]. \tag{22}$$

Using a typical value of 0.025 $(\text{V-cm})^{0.5}$ for $\beta$, the Poole–Frenkel constant, the experimental value of $E_t$, and, as above, $E = 10$ V/cm, we obtain $n_f/n_t = 0.0014$ at room temperature. Thus TRDL signals observed experimentally on $TiO_2$ nanoparticles must arise from only a very small fraction of the charge carriers generated by photoexcitation; yet, like the proverbial tip of the iceberg, they enable us to monitor the dynamics of the whole carrier population. Accordingly the results of Martin and coworkers[52] actually measure the lifetime, as $\tau_1$, of the deep-trapped electron, i.e., Ti(III) states.

Taken together with the spectroscopic results, the TRDL data also enable us to propose a mechanism for photocatalytic silver reduction by single electron transfer from Ti(III) to Ag(I)

$$\text{Ti(III)} + \text{Ag(I)} \rightarrow \text{Ti(IV)} + \text{Ag}^{\circ} \tag{23}$$

The Ti(III) surface states thus represent the latent image in photocatalytic imaging. Equation 23 is inconsistent with the earlier electrochemical models,[48] which assumed reduction of silver ion by conduction band electrons. The microsecond lifetime for the Ti(III) states also suggests that efficient photocatalytic silver recovery can be practiced on effluents wherein the silver ion concentration is as low as $10^{-4}$ M, consistent with the experimental results of Herrmann and coworkers.[46]

## Conclusions

The power of the TRDL technique to provide useful information on photoconducting materials for electrophotographic and photocatalytic applications has been illustrated by the following examples:

1. A TRDL study of Cu-doped CdS powders[22,23] illustrated the particular utility of temperature variation, which allowed us to identify the (sulfide vacancy) donor state intermediate in generating free conduction band photoelectrons, as well as postulate a double minimum potential energy surface for hole trapping at the Cu(I) centers. An analysis of the kinetics of TRDL signal decay supported a model in which hole trapping was rate determining for recombination. Temperature-dependent TRDL also revealed a continuum of deep electron trapping states near the Fermi level of CdS; the density of these states was correlated with Canongraphic imaging performance.
2. As a model of a two-component photoreceptor, the system undoped CdS dispersed in a xylene solution of phenylhydrazine was studied by TRDL.[31,32] The phenylhydrazine provides a pathway for surface recombination. Varying the substituent on the phenylhydrazine (and hence, its ionization potential) allowed us to establish that the rate-limiting step in recombination occurs in the Marcus normal energy regime, and that photohole capture by the adsorbate is rate determining. Determining the activation parameters as well as the rate constant for surface recombination in this case allowed us to estimate the electrochemical transfer coefficient, hence the ambipolar charge separation distance at the beginning of charge carrier diffusion or drift.
3. We reviewed the work of Smit and Warman[43] on model molecular charge-generating species. It demonstrates that TRDL is useful to probe charge separation occurring over molecular distances and can lead to a figure of merit for evaluating potential molecular charge generating components for electrophotographic application.
4. Dichotomies in the mechanisms of photocatalytic imaging and of photocatalytic silver recovery from solution, both employing nanocrystalline $TiO_2$ as the photoactive species, were resolved, in part, by TRDL studies.[51,52] These studies confirm that the latent image in photocatalytic imaging comprises Ti(III) surface states on $TiO_2$. The system $TiO_2$-silver is of particular interest as an example of how the sensitivity of TRDL measurement to only a small fraction of the photogenerated charge carriers enables the dynamics of the whole carrier population to be monitored.

**Acknowledgment.** Figures 2 through 6 are taken from Refs. 22 and 23, and are reproduced with kind permission of the copyright holder, the American Institute of Physics. We thank Dr. John M. Warman and Dr. Susan S. Collier for helpful discussions in the course of the original work in our laboratories, as reviewed in this article. The interest and encouragement of Prof. N. Serpone are acknowledged with gratitude.

## References

1. J. Heieck, in *Proceedings of IS&T's 49th Annual Conference*, Springfield, VA, 1996.
2. Th. Müssig, *J. Imaging Sci. Technol.* **41**: ~~118–127~~ (1997).
3. (a) M. P. DeHaas and J. M. Warman, *Chem. Phys.* **73**: 35 (1982); (b) J. M. Warman, M. P. DeHaas, P. Pichat, T. P. M. Koster, E. A. van der Zouwen-Assink, A. Mackor, and R. Cooper, *Radiat. Phys. Chem.* **37**: 433 (1991).
4. R. P. Deri and J. P. Spoonhower, *Photogr. Sci. Eng.* **28**: 92 (1984).
5. J. M. Warman, in *The Study of Fast Processes and Transient Species by Pulse Radiolysis*, J. H. Baxendale and F. Busi, Eds., Riedel, Dordrecht, 1982, pp. 129-161.
6. W. H. Hartwig and J. J. Hinds, *J. Appl. Phys.* **40**: 2020 (1969).
7. B. Kramer, S. Gelfman and L. Kalikstein, *Phys. Rev. B* **6**: 556 (1972).
8. S. S. Collier, A. K. Weiss and R. F. Reithel, *Photogr. Sci. Eng.* **20**: 54 (1976).
9. S. Ishihara, *Electrophotogr.* **20**: 17 (1982).
10. S. Faria and R. E. Karam, *J. Appl. Photogr. Eng.* **8**: 245 (1982).
11. (a) J. W. Shepard, *J. Appl Photogr. Eng.* **8**: 210 (1982); (b) C. Zou, M. R. V. Sahyun, B. Levy, and N. Serpone, *J. Imaging Sci. Technol.* **40**: 94 (1996).
12. J. J. A. Robillard, Fr. Patent 2,254,047 (1973); *Photogr. Sci. Eng.* **8**: 18 (1964).
13. (a) H. Jonker,C. J. Kippel, H. J. Hutman, J. G. F. Janssen, and L. K. H. van Beek, *Photogr. Sci. Eng.* **13**: 1 (1969); (b) E. Berman, *ibid.* **13**: 50 (1969); (c) G. L. McLeod, *ibid.* **13**: 93 (1969); (d) H. Tabei and S. Nara, Japanese Patent 73,114,370 (1973).
14. M. R. V. Sahyun, *J. Imaging Sci.* **33**: 94 (1989).
15. B. Levy, in *IS&T Symposium on Electronic and Ionic Properties of Silver Halides: Common Trends with Photocatalysis*, Springfield, VA, 1991.
16. R. A. Bogomolni, H. Tributsch, G. Petermann, and M. P. Klein, *J. Chem. Phys.* **78**: 2579 (1983).
17. M. R. V. Sahyun, *Chem. Phys. Lett.* 112: 571 (1984); *Electrochim. Acta* **30**: 619 (1985).
18. H. Herrmann, S. T. Martin and M. R. Hoffmann, *J. Phys. Chem.* **99**: 16641 (1995).
19. J. W. Weigl, *ACS Symp. Ser.* **200**: 139 (1982); *Angew. Chem.* **89**: 386 (1977).
20. R. L. Shaffert, *Electrophotography*, Focal Press, London, 1975, pp 111ff.
21. (a) R. Clasen, *J. Photogr. Sci.* **28**: 226 (1980); H. Hirsch, *ibid.* **25**: 60 (1977); (b) O. L. Nelson and D. M. Korn, *Photogr. Sci. Eng.* **22**: 189 (1978).
22. D. H. Klosterboer, W. L. Meissner and M. R. V. Sahyun, *J. Appl. Phys.* **54**: 5161 (1983).
23. G. H. Dierssen and M. R. V. Sahyun, *J. Appl. Phys.* **56**: 1647 (1984).
24. J. Woods and K. H. Nicholas, *Br. J. Appl. Phys.* **15**: 1361 (1964).
25. G. Düssel and K. W. Boer, *Phys. Status Solidi* **59**: 375, 391 (1970).
26. M. R. V. Sahyun and R. G. Brisbois, *J. Appl. Phys.* **59**: 2189 (1986).
27. T. C. McGill, *J. Vac. Sci. Technol.* **11**: 935 (1974).
28. (a) J. Mort and G. Pfister, in *Electronic Properties of Polymers*, J. Mort and G. Pfister, Eds., Wiley, New York, 1982, Chap. 6; (b) H. B‰ssler, *Phys. Stat. Sol.* **107**: 9 (1981).

29. (a) M. E. Scharfe, D. M. Pai and R. J. Gruber, in *Imaging Materials and Processes*, 8th ed., J. M. Sturge, V. Walworth and A. Shepp, Eds., Van Nostrand-Reinhold, New York, 1989, chap. 5; (b) L. B. Schein, *Electrophotography and Development Physics*, 2nd ed., Springer-Verlag, Berlin, 1992, pp. 29ff.; (c) M. B. O'Regan, P. M. Borsenberger, E. H. Magin, and T. Zubil, *J. Imaging Sci. Technol.* **40**: 1 (1996).
30. W. J. Dullmage, W. A. Light, S. J. Marino, C. D. Salzburger, D. L. Smith, and W. J. Studenmayer, *J. Appl. Phys.* **49**: 5543 (1978); P. Borsenberger, A. Chowdry, D. C. Hoesterey, and W. Mey, *ibid*. 49: 5555 (1978).
31. M. R. V. Sahyun, *Chem. Phys. Lett.* **121**: 469 (1985).
32. M. R. V. Sahyun, in *Unconventional Photoactive Solids*, H. Scher, Ed., Plenum, New York, 1988, p. 133.
33. M. R. V. Sahyun, *J. Appl. Phys.* **61**: 3044 (1987).
34. (a) C. Levy-Clement, in *Photochemical Energy Conversion*, J. R. Norris, Jr., and D. Meisel, Eds., Elsevier, New York, 1989, pp. 267ff.; (b) N. Serpone, *ibid*., pp. 297ff; (c) E. Amouyal and B. Zidler, *Isr. J. Chem.* **22**: 117 (1982).
35. L. P. Hammett, *Physical Organic Chemistry*, McGraw-Hill, New York, 1940, chap. 7.
36. (a) H. C. Brown and Y. Okamoto, *J. Am. Chem. Soc.* **80**: 4979 (1958); (b) A. G. Harrison, P. Kebarle, and F. P. Lossing, *ibid.* **83**: 777 (1961).
37. R. W. Taft, Jr., and I. C. Lewis, *J. Am. Chem. Soc.* **81**: 5343 (1959).
38. R. A. Marcus, *Ann. Rev. Phys. Chem.***15**: 155 (1954); *Electrochim. Acta* **13**: 995 (1968).
39. N. Agmon and R. D. Levine, *Isr. J. Chem.* **19**: 330 (1980).
40. (a) R. M. Gibb, G. J. Rees, B. W. Thomas, B. L. H. Wilson, B. Hamilton, D. R. Wright, and N. F. Mott, *Phil. Mag.* **36**: 1021 (1977); (b) J. F. Hamilton, *Photogr. Sci. Eng.* **27**: 225 (1984).
41. R. R. Dogonadze, in *Reactions of Molecules at Electrodes*, N. S. Hush, Ed., Wiley-Interscience, London, 1971; see also Ref. 42b.
42. (a) W. F. Leonard and T. L. Martin, Jr., *Electronic Structure and Transport Properties of Crystals*, Krieger, Huntington, NY, 1980, pp. 630ff.; (b) V. G. Levich, in *Physical Chemistry: an Advanced Treatise*, vol. IXb, H. Eyring, Ed., Academic Press, New York, 1970, chap. 12; (c) H. Eyring, *J. Chem. Phys.* **3**: 107 (1935).
43. K. J. Smit and J. M. Warman, *J. Luminesc.* **42**: 149 (1988).
44. M. D. Tabak, D. M. Pai and M. E. Scharfe, *J. Non-Cryst. Solids* **6**: 357 (1971).
45. M. R. V. Sahyun, *Photogr. Sci. Eng.* **28**: 185 (1984).
46. J.-M. Herrmann, J. Disdier and P. Pichat, *J. Catal.* **113**: 72 (1988).
47. H. Tahiri and N. Serpone, *J. Adv. Oxid. Technol.* **1**: 179 (1996).
48. (a) P. D. Fleischauer, H. K. A. Kan and J. R. Shepard, *J. Am. Chem. Soc.* **94**: 283 (1972); (b) H. Hada, Y. Yonezawa, M. Ishino, and H. Tanemura, *J. Chem. Soc. Faraday Trans.* **78**: 2677 (1982); (c) H. Hada, Y. Yonezawa and M. Saikawa, *Bull. Chem. Soc. Japan* **55**: 2010 (1982).
49. A. J. Nozik and R. Memming, *J. Phys. Chem.* **100**: 13,064 (1996) and references cited therein.
50. N. Serpone, D. Lawless, R. Khairutdinov, and E. Pellizzetti, *J. Phys. Chem.* **99**: 16,655 (1995).
51. J. M. Warman, M. P. de Haas, P. Pichat, and N. Serpone, *J. Phys. Chem.* **95**: 8858 (1991).
52. S. T. Martin, H. Herrmann and M. R. Hoffmann, *J. Chem. Soc. Faraday Trans.***90**: 3323 (1994).
53. M. R. V. Sahyun and N. Serpone, *Langmuir*, accepted for publication.
54. J. Frenkel, *Phys. Rev.* **54**: 647 (1938).